

# Docking-Based Investigation of Synthesized Heterocyclic Compounds for Antifungal and Antitubercular Potential

Mr. Deepak P. Gavate<sup>1\*</sup>, Dr. Vilas L. Badgujar<sup>2</sup>, Dr. Bhupendra L. Deore<sup>3</sup>,  
Mr. Chetan V. Jain<sup>4</sup>, Mr. Vivek B. Patil<sup>5</sup>

*DCS's A.R.A College of Pharmacy Nagaon, Dhule-424 005(MH)<sup>1\*</sup>,  
Professor & HOD of Quality Assurance DCS's A.R.A College of Pharmacy Nagaon, Dhule-  
424 005(MH)<sup>2</sup>,  
Associate Professor of Quality Assurance DCS's A.R.A College of Pharmacy Nagaon, Dhule-  
424 005(MH)<sup>3</sup>,  
Assistant Professor of Pharmaceutics DCS's A.R.A College of Pharmacy Nagaon, Dhule-424  
005(MH)<sup>4</sup>,  
Assistant Professor of Quality Assurance DCS's A.R.A College of Pharmacy Nagaon, Dhule-  
424 005(MH)<sup>5</sup>*  
[gavatedeepak.210@gmail.com](mailto:gavatedeepak.210@gmail.com)<sup>1\*</sup>, [vilaspharma007@gmail.com](mailto:vilaspharma007@gmail.com)<sup>2</sup>, [bhupendradeore@gmail.com](mailto:bhupendradeore@gmail.com)<sup>3</sup>,  
[cvj5395@gmail.com](mailto:cvj5395@gmail.com)<sup>4</sup>, [vivekpatil2799@gmail.com](mailto:vivekpatil2799@gmail.com)<sup>5</sup>

## Abstract

*This pressing need for novel, potent antimicrobial drugs has been highlighted by the growing resistance of Mycobacterium TB strains and fungal infections to current treatments. This work used molecular docking techniques to synthesis a number of new heterocyclic compounds and assess their antifungal and antitubercular capabilities. For antifungal activity, the key target proteins were yeast Sec14p (PDB ID: 6F0E) and catalase-peroxidase KatG (PDB ID: 1U2J); for antitubercular evaluation, the key target proteins were InhA (isoniazid target, PDB ID: 1ENY) and anthranilate phosphoribosyltransferase (trpD, PDB ID: 3R6C). PyRx was used for docking simulations, while Biovia Discovery Studio was used to visualize binding interactions. I-MB2 outperformed common medications like fluconazole and isoniazid, showing the greatest binding affinities of  $-10.4$  kcal/mol (6F0E) and  $-10.6$  kcal/mol (1ENY) among the substances studied. Additionally, compounds B-MB3 and I-MB3 showed encouraging multi-target activity. According to these results, the produced heterocyclic derivatives—in particular, I-MB2—represent promising candidates for the creation of medicines with dual antifungal and antitubercular properties.*

**Keywords:** Heterocyclic compounds, Molecular docking, PyRx, Antifungal activity, Antitubercular activity, Binding affinity, Isoniazid, Fluconazole, 1U2J, 6F0E, 1ENY, 3R6C

## 1. Introduction

Globally, infectious illnesses remain a significant public health problem, particularly in underdeveloped countries with inadequate access to high-quality healthcare. Among them, fungal infections and tuberculosis (TB) are especially dangerous since they are becoming more resistant to current therapies.[1],[2],[3] The extremely infectious bacterial infection known as tuberculosis (TB), which is mostly affecting the lungs but may also spread to other regions of the body, is caused by *Mycobacterium tuberculosis*. Approximately 10.6 million individuals contracted tuberculosis (TB) in 2022, and 1.3 million of those cases resulted in death, according to the World Health Organization (WHO). [4] Accordingly, tuberculosis is one of the top 10 causes of mortality worldwide. Despite the availability of medications such as isoniazid, therapy has become more challenging due to the advent of extensively drug-resistant (XDR) and multidrug-resistant (MDR) TB strains.

Conversely, fungal infections are on the rise and are getting worse, particularly in those with compromised immune systems, such as cancer patients, transplant recipients, and HIV/AIDS patients. Common fungal pathogens that cause potentially fatal infections include *Aspergillus* species, *Cryptococcus* species, and *Candida* species. [5],[6],[7] These fungi can result in high fatality rates by causing systemic infections that are challenging to identify and cure. Even though fluconazole and other antifungal medications are often used, many fungal strains are becoming resistant, which makes conventional treatments less effective. Additionally, invasive fungal infections are difficult to diagnose since they frequently resemble other illnesses and need specific laboratory tests.

All things considered, TB and fungal diseases both emphasize how urgently new, more potent treatment medicines are needed. Research into new chemicals and cutting-edge drug design techniques has grown in significance due to rising resistance and a lack of available medications. By forecasting how they will interact with biological targets, contemporary methods like molecular docking can assist in the identification of prospective drug candidates. This strategy is essential for creating therapies that can go past the present restrictions in antifungal therapy and tuberculosis.

### Need for Novel Therapeutic Agents

Even while medications like fluconazole for fungal infections and isoniazid for tuberculosis are readily available, their treatment effectiveness is hindered by the development of drug-resistant strains, side effects, and long-term toxicity. [8], [9], [10] Many current medications are no longer as effective due to extensively drug-resistant TB (XDR-TB) and multidrug-resistant TB (MDR-TB), which calls for the development of novel chemical entities with enhanced safety, potency, and selectivity. [11], [12] Similarly, increasing reports of azole-resistant *Candida* species call for the development of new antifungal scaffolds. [13], [14]

### Importance of Heterocyclic Compounds in Drug Design

In medicinal chemistry, heterocyclic compounds—especially those with nitrogen, sulfur, and oxygen atoms—are favored scaffolds because of their structural variety, stability, and biological compatibility. [15],[16] Heterocycles are the basis for several FDA-approved

medications, such as antibacterial, antiviral, antifungal, antitubercular, anticancer, and anti-inflammatory treatments. [17],[18], [19] In earlier research, compounds of thiazolidinone, oxadiazole, pyrazole, benzothiazole, and quinoline shown exceptional antibacterial and antimycobacterial capabilities. [20], [21], [22]

### **Molecular Docking as a Predictive Tool**

Computational techniques like molecular docking have greatly aided modern drug development procedures by enabling quick and economical screening of possible therapeutic candidates. [23]. The binding orientation, interaction pattern, and binding affinity of a chemical within a biological target's active site may be predicted via molecular docking. Understanding structure-activity relationships (SAR), finding lead compounds, and increasing the effectiveness of medication design can all be aided by this knowledge. [24], [25]

Molecular docking experiments were used to assess the antitubercular and antifungal properties of a number of new heterocyclic compounds that were produced in this study. Molecular docking is a computer method that predicts how well tiny molecules (ligands) connect to biological targets (enzymes or receptors), revealing information about the type and strength of the interactions. [26]. When screening and ranking active chemicals for additional biological testing, this approach is quite helpful.

The produced compounds were contrasted with the common antitubercular medication Isoniazid in order to evaluate the antitubercular potential using docking experiments against a validated target protein implicated in *M. tuberculosis* survival. [27] Similarly, fungal enzyme targets that are pertinent to *Candida* species were used for docking in order to assess antifungal activity, and comparisons with the common antifungal medication Fluconazole were done. [28]

### **Research Objectives**

In this study, a series of novel heterocyclic compounds were synthesized and evaluated for their potential as antifungal and antitubercular agents using molecular docking studies. The synthesized molecules were docked against well-validated biological targets relevant to TB and fungal infections, and their binding affinities were compared with standard drugs— Isoniazid for antitubercular and Fluconazole for antifungal activity. The goal was to identify candidates with superior or comparable binding profiles, indicating promising biological activity.

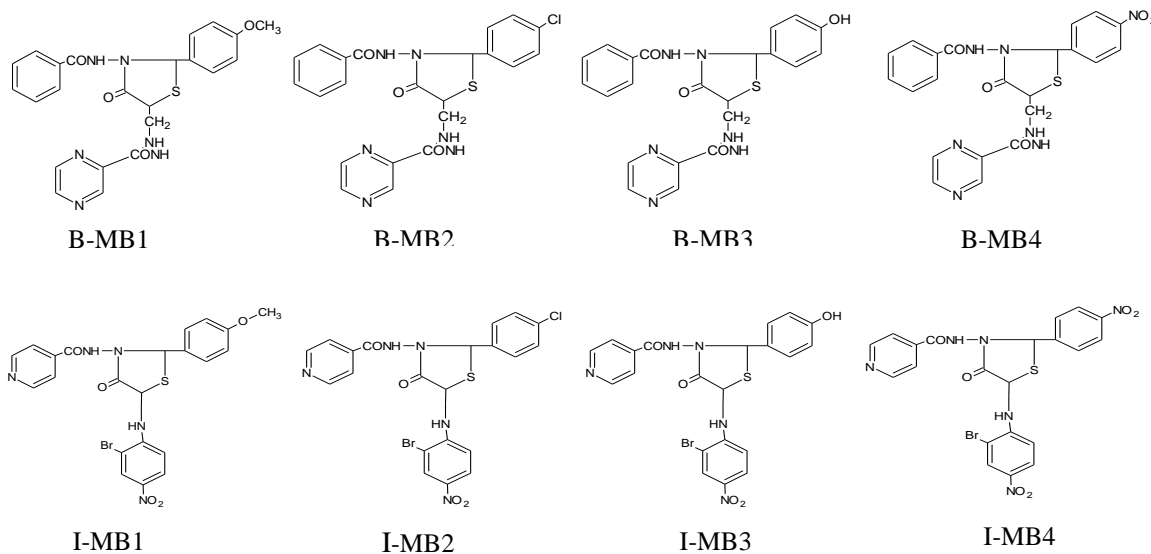
This approach not only aids in identifying lead compounds for further *in vitro* and *in vivo* studies but also contributes to the ongoing search for more effective treatments against drug-resistant infections.

## **2. Materials and Methods**

### **2.1 Chemical Synthesis of Heterocyclic Compounds**

Standard organic synthesis techniques were used to create a number of heterocyclic derivatives. Schiff bases were created by condensation of suitable aldehydes with hydrazides, while thiazolidinones and other heterocyclic frameworks were produced by cyclization processes. Using the appropriate solvent systems, thin-layer chromatography (TLC) was used to monitor every reaction. Recrystallization or column chromatography were used to purify the produced

compounds, and spectrum methods including infrared,  $^1\text{H-NMR}$ ,  $^{13}\text{C-NMR}$ , and mass spectrometry were used to validate their structures.



## 2.2 Selection of Target Proteins

Protein structures from the RCSB Protein Data Bank (PDB) that are pertinent to mycobacterial and fungal viability were chosen for the docking investigation. In particular:

- For antifungal action, use the C-terminal domain of yeast Sec14p with a picolinamide molecule PDB ID: 6F0E and the catalase-peroxidase KatG of Escherichia coli PDB ID: 1U2J.
- For antitubercular activity: Mycobacterium tuberculosis isoniazid target PDB ID: 1ENY & Structure of Mycobacterium tuberculosis Anthranilate Phosphoribosyltransferase (trpD) (complex with inhibitor ACS179) ID of PDB: 3R6C

## 2.3 ADME Prediction Test

The ADME prediction test analyzed in the Swiss ADME application provides insights into the physicochemical properties and pharmacokinetic activities of several compounds, particularly metabolites from *synthesized derivative* in conjunction with standard drugs (Fluconazole and Isoniazid).

### 2.3.1 Physiochemical Activity

This table delineates the structural attributes of each compound, including the quantity of heavy atoms, aromatic heavy atoms, proportion of  $\text{sp}^3$  carbons, and molar refractivity. These qualities can offer information into a compound's stability and potential reactivity within biological systems. For instance, I-MB4 exhibits the highest molar refractivity (141.50) suggesting its potentially greater molecular size and polarity in comparison of standard drug such as Fluconazole and Isoniazid. (Table 1).

### 2.3.2 Lipophilicity

Lipophilicity is represented by the logarithm of the octanol-water partition coefficient (Log P), a crucial determinant of a compound's ability to traverse biological membranes, such as the

blood-brain barrier. chemicals with high lipophilicity tend to concentrate in adipose tissues, whereas hydrophilic chemicals demonstrate greater solubility in water. I-MB2 & I-MB4 exhibits significant lipophilicity (Log P ~ -1.24), but Fluconazole & Isoniazid possesses a moderate Log P of 0.41 & 0.03, indicating it may be absorbed more readily. (Table 2).

### 2.3.3 Water Solubility

This table presents estimates of the solubility of each substance in water, represented as Log S (solubility). Water solubility is essential for the absorption of pharmaceuticals in the body. Isoniazid exhibits exceptional solubility, facilitating its absorption in the gastrointestinal tract. Conversely, B-MB3 & B-MB4 exhibit limited solubility, potentially impeding their absorption and efficacy as therapeutic agents until solubility is improved (Table 3).

### 2.3.4 Pharmacokinetic Activity

This section examines the chemicals' behavior in biological systems concerning absorption, distribution, metabolism, and excretion. For instance, B-MB1 - B-MB4 & I-MB1 - I-MB4 is extensively absorbed in the gastrointestinal system; yet, it does not penetrate the blood-brain barrier (BBB) and is not a substrate of P-glycoprotein (P-gp), indicating a reduced likelihood of being discharged by cellular efflux pumps. I-MB1 & I-MB2 characterized by low gastrointestinal absorption and skin permeability, may encounter obstacles in therapeutic applications; however, they could be changed to enhance their pharmacokinetic features (Table 4).

**Table 1: ADME prediction & Physiochemical activity**

Compound	Physiochemical Activity							
	Num. Heavy Atoms	Num. Arom. Heavy Atoms	Fractio n Csp3	Num. Rotatable Bonds	Num. H-bond Acceptors	Num. H-Bond Donor	Molar Refractivity	TPSA
B-MB1	34	18	0.21	8	6	2	127.47	166.80 Å <sup>2</sup>
B-MB2	33	18	0.14	7	5	3	124.15	169.60 Å <sup>2</sup>
B-MB3	33	18	0.14	7	6	4	121.16	189.83 Å <sup>2</sup>
B-MB4	35	18	0.14	8	7	3	127.96	215.42 Å <sup>2</sup>
I-MB1	35	18	0.17	8	6	2	139.17	168.67 Å <sup>2</sup>
I-MB2	34	18	0.14	7	5	2	137.69	159.44 Å <sup>2</sup>
I-MB3	34	18	0.14	7	6	3	134.70	179.67 Å <sup>2</sup>
I-MB4	36	18	0.14	8	7	2	141.50	205.26

								Å <sup>2</sup>
Fluconazole	22	16	0.23	5	7	1	70.71	81.65 Å <sup>2</sup>
Isoniazid	10	6	0.00	2	3	2	35.13	68.01 Å <sup>2</sup>

Table 2: Lipophilicity of the compound

Compound	Lipophilicity					
	Log Po/w (iLOGP)	Log Po/w (XLOGP3)	Log Po/w (WLOGP)	Log Po/w (MLOGP)	Log Po/w (SILICO-SIT)	Consensus Log Po/w
B-MB1	-15.02	2.39	1.93	1.65	1.85	-1.44
B-MB2	-9.79	2.45	1.60	1.44	1.25	-0.61
B-MB3	-15.14	1.47	0.66	0.46	0.13	-2.49
B-MB4	-13.09	1.65	0.86	0.16	-1.53	-2.39
I-MB1	-7.24	4.33	3.24	1.73	0.76	0.56
I-MB2	-1.24	4.98	3.89	2.50	1.33	2.29
I-MB3	-1.64	4.00	2.94	1.52	0.21	1.41
I-MB4	-1.24	4.18	3.14	1.22	-1.45	1.17
Fluconazole	0.41	0.35	1.47	1.47	0.71	0.88
Isoniazid	0.03	-0.70	-0.31	-0.47	-0.27	-0.35

Table 3: Water solubility of the compound

Compound	Water Solubility		
	Log S (ESOL)	Log S (Ali)	Log S (ESOL)
B-MB1	-4.18 3.15e-02 mg/ml ; 6.57e-05 mol/l Moderately soluble	-4.81 1.40e-03 mg/ml ; 2.92e-06 mol/l Moderately soluble	-6.36 2.09e-04 mg/ml ; 4.37e-07 mol/l Poorly soluble
B-MB2	-4.33 2.26e-02 mg/ml ; 4.66e-05 mol/l Moderately soluble	-5.66 1.07e-03 mg/ml ; 2.21e-06 mol/l Moderately soluble	-6.49 2.24e-04 mg/ml ; 4.59e-07 mol/l Poorly soluble
B-MB3	-3.60 1.17e-01 mg/ml ; 2.51e-04	-5.06	-5.32

	mol/l soluble	4.03e-03 mg/ml ; 8.65e-06 mol/l Moderately soluble	2.24e-03 mg/ml ; 4.81e-06 mol/l Moderately soluble
B-MB4	-3.80 7.78e-02 mg/ml ; 1.57e-04 mol/l soluble	-5.79 8.09e-04 mg/ml ; 1.63e-06 mol/l Moderately soluble	-5.24 2.84e-03 mg/ml ; 5.74e-06 mol/l Moderately soluble
I-MB1	-5.89 7.23e-04 mg/ml ; 1.29e-06 mol/l Moderately Soluble	-7.59 1.45e-05 mg/ml ; 2.59e-08 mol/l Poorly soluble	-6.92 6.68e-05 mg/ml ; 1.19e-07 mol/l Poorly soluble
I-MB2	-6.40 2.23e-04 mg/ml ; 3.95e-07 mol/l Poorly soluble	-8.07 4.83e-06 mg/ml ; 8.57e-09 mol/l Poorly soluble	-7.41 2.21e-05 mg/ml ; 3.93e-08 mol/l Poorly soluble
I-MB3	-5.67 1.16e-03 mg/ml ; 2.13e-06 mol/l Moderately soluble	-7.48 1.83e-05 mg/ml ; 3.35e-08 mol/l Poorly soluble	-6.24 3.15e-04 mg/ml ; 5.78e-07 mol/l Poorly soluble
I-MB4	-5.88 7.63e-04 mg/ml ; 1.33e-06 mol/l Moderately soluble	-8.20 3.63e-06 mg/ml ; 6.32e-09 mol/l Poorly soluble	-6.16 4.01e-04 mg/ml ; 6.98e-07 mol/l Poorly soluble
Fluconazole	-2.17 2.08e+00 mg/ml ; 6.80e-03 mol/l soluble	-1.63 7.20e+00 mg/ml ; 2.35e-02 mol/l Very soluble	-3.54 8.83e-02 mg/ml ; 2.88e-04 mol/l soluble
Isoniazid	-0.56 3.77e+01 mg/ml ; 2.75e-01 mol/l Very soluble	-0.25 7.66e+01 mg/ml ; 5.58e-01 mol/l Very soluble	-1.64 3.17e+00 mg/ml ; 2.31e-02 mol/l soluble

Table 4: Pharmacokinetic activity of the compound

Compound	Pharmacokinetic Activity								
	GI Absorption	BBB Permeant	P-gp substrate	CYP1 A2 Inhibitor	CYP2 C9 Inhibitor	CYP2 D6 Inhibitor	CYP2 A4 Inhibitor	CYP3 Inhibitor	Log K <sub>p</sub> (skin permeation)
B-MB1	Low	No	Yes	No	No	No	No	No	-7.53 cm/s
B-MB2	Low	No	Yes	No	Yes	No	No	No	-7.52 cm/s
B-MB3	Low	No	Yes	No	No	No	No	No	-8.10 cm/s
B-MB4	Low	No	Yes	No	No	No	No	No	-8.15 cm/s
I-MB1	Low	No	Yes	No	Yes	No	No	No	-6.64 cm/s
I-MB2	Low	No	Yes	No	Yes	Yes	No	Yes	-6.20 cm/s
I-MB3	Low	No	Yes	No	Yes	No	No	Yes	-6.79 cm/s
I-MB4	Low	No	Yes	No	Yes	Yes	No	Yes	-6.84 cm/s
Fluconazole	High	No	Yes	No	Yes	No	No	No	-7.92 cm/s
Isoniazide	High	No	No	No	No	No	No	No	-7.63 cm/s

## 2.4 Preparation of Protein

The following steps were taken to get the protein ready for molecular docking studies:

- 1. Downloading the Protein Structure:** To ensure that it contained the protein and the bound ligand, the PDB file with PDB IDs 1U2J, 6F0E, 1ENY, and 3R6C was downloaded.
- 2. Eliminating Undesired Molecules:** A clean structure was obtained by examining the downloaded protein structure. Heteroatoms, co-crystallized ligands, and water molecules were removed. To guarantee that the docking experiments only concentrate on the target protein and are not influenced by other factors, this step is essential.
- 3. Energy Minimization:** To minimize steric conflicts and maximize the protein's structure, we carried out energy minimization. Prior to docking, the protein's structure was fine-tuned

using a molecular dynamics simulation.

**4. Protein Structure Validation:** Using validation algorithms that look for geometric and energetic consistency, we evaluated the generated protein structure's quality. This stage guarantees that the protein model is appropriate for trustworthy docking investigations.

### 2.5 Preparation of Ligands

Using ChemDraw, the synthesized compounds were shown, and Chem3D was used to transform them into three-dimensional structures. After that, the ligand files were stored in PDB format and transformed for docking into PDBQT format.

## 3. Molecular docking test

PyRx software was utilized for the molecular docking studies. PyRx software was used to generate the study's findings. They showed the mode, RMSD lower limit, upper limit, and binding affinity expressed in kcal/mol. A chemical is said to have a tendency to create bonds with the target protein if its binding affinity value is low. When a compound's binding affinity rises, less energy is required to create bonds. As a result, a chemical will be more likely to attach to the target protein. The established bonds' variability is shown by the mode parameter. The computed forecasts' accuracy and precision are shown by the RMSD metric. Compounds with a low binding affinity value often show perfect properties in the RMSD lower bound and zero upper bound modes. By examining the docking data, we were able to characterize the location, kind, and number of bonds formed between the test chemical and the target protein. The visualization technique makes use of the Biovia program. Integrating the docked conformation into the target protein allows us to see it. It is therefore possible to determine the location, kind, and amount of bonds that were created.

### 3.1 Python Prescription (PyRx)

For structure-based virtual screening in drug development, PyRx is an easy-to-use application. It enables users to create a workspace in which all project files and output are arranged nicely. Protein structures and ligand libraries may be imported into the program in PDB format, and it will automatically convert them into the PDBQT format needed for docking. During this conversion, PyRx detects rotatable bonds in ligands and adds atomic charges. By moving a grid box across the binding pocket, users may utilize the 3D viewer to determine the protein's active site. Next, the Vina Wizard assists in configuring docking parameters including number of poses, exhaustiveness, and ligand selection. PyRx uses AutoDock Vina or AutoDock 4 to predict binding affinities and postures after docking has begun. For additional investigation, the findings may be exported in PDBQT, SMILES, or CSV formats after being sorted and displayed. (Table 5)

**Table 5: Docking layout parameter**

SR. NO	A) 1U2J	B) 6F0E	C) 1ENY	D) 3R6C
<b>GRID PARAMETERS (X, Y ,Z )</b>	X – 64.4768 Y – 41.8423 Z – 49.7465	X – 60.5303 Y – 46.3934 Z – 52.9203	X - 65.3450 Y – 41.8621 Z – 90.1321	<b>X – 60.1139</b> <b>Y – 47.8748</b> <b>Z - 52.9916</b>
<b>CENTER</b>	<b>48.6205</b> <b>109.6701</b> <b>90.1294</b>	<b>35.3791</b> <b>13.1845</b> <b>-20.6889</b>	<b>48.5831</b> <b>109.6594</b> <b>90.1321</b>	<b>35.2886</b> <b>12.4075</b> <b>-20.7383</b>

## 4. RESULTS

### 4.1 Molecular docking test result for Antifungal activity

The binding interactions of produced chemicals against the fungal gene "catalase-peroxidase KatG" of Escherichia coli (P21 21 21) PDB ID: 1U2J and yeast Sec14p with picolinamide PDB ID: 6F0E were assessed using a molecular docking approach. These metabolites were compared to common antifungal medications like fluconazole in terms of their binding affinities (in kcal/mol). (Table 6)

**Table 6: Docking test of Antifungal activity**

Compound	PDB ID: 1U2J				PDB ID: 6F0E			
	Binding Affinity (kcal/mol)	RMSD lower bound	RMSD upper bound	Mode	Binding Affinity (kcal/mol)	RMSD lower bound	RMSD upper bound	Mode
<b>B-MB<sub>1</sub></b>	-6.8	0.0	0.0	0	-8.5	0.0	0.0	0
<b>B-MB<sub>2</sub></b>	-6.9	0.0	0.0	0	-8.5	0.0	0.0	0
<b>B-MB<sub>3</sub></b>	-6.7	0.0	0.0	0	-7.9	0.0	0.0	0
<b>B-MB<sub>4</sub></b>	-7.9	0.0	0.0	0	-8.8	0.0	0.0	0
<b>I- MB<sub>1</sub></b>	-6.6	0.0	0.0	0	-8.3	0.0	0.0	0
<b>I- MB<sub>2</sub></b>	-7.9	0.0	0.0	0	-10.4	0.0	0.0	0
<b>I- MB<sub>3</sub></b>	-7.6	0.0	0.0	0	-8.8	0.0	0.0	0
<b>I- MB<sub>4</sub></b>	-7.5	0.0	0.0	0	-9	0.0	0.0	0
<b>Std. Fluconazole</b>	-6.4	0.0	0.0	0	-7.1	0.0	0.0	0

#### 4.1.1 Evaluation of outcomes

To assess the synthetic test ligands' antifungal ability, they were docked against the fungal gene targets PDB IDs 1U2J and 6F0E. Between -6.7 and -6.9 kcal/mol, compounds B-MB1 through B-MB3 had somewhat higher binding affinities against 1U2J than fluconazole. Between -7.5 and -7.9 kcal/mol, compounds B-MB4 and I-MB1 showed much greater affinity to I-MB4. This implies that a few of these substances could inhibit 1U2J more potently than fluconazole. Superior binding affinities ranging from -7.9 to -10.4 kcal/mol were demonstrated by all test compounds (B-MB1 to B-MB4 and I-MB1 to I-MB4) when docked against 6F0E. At -10.4 kcal/mol, I-MB2 notably showed the greatest binding. These findings suggest that the test compounds—I-MB2 in particular—may have more potent antifungal action than fluconazole. These synthetic ligands have the potential to be effective antifungal medicines, according to the docking research.

#### 4.2 Molecular docking test result for Antitubercular activity

The crystal structure and function of the isoniazide target of Mycobacterium tuberculosis PDB ID: 1ENY and anthranilate phosphoribosyltransferase (trpD) from Mycobacterium tuberculosis PDB ID: 3R6C were examined in a molecular docking study to assess the binding interactions of synthesized compounds against the TB gene. These metabolites' binding affinities (measured in kcal/mol) were contrasted with those of common antifungal medications like isoniazide. (Table 7)

**Table 7: Docking test of Antitubercular activity**

Compound	PDB ID: 1ENY				PDB ID: 3R6C			
	Binding Affinity (kcal/mol)	RMS D lower bound	RMS D upper bound	Mode	Binding Affinity (kcal/mol)	RMS D lower bound	RMS D upper bound	Mode
<b>B-MB<sub>1</sub></b>	-9.4	0.0	0.0	0	-8.8	0.0	0.0	0
<b>B-MB<sub>2</sub></b>	-9.5	0.0	0.0	0	-8.5	0.0	0.0	0
<b>B-MB<sub>3</sub></b>	-9.6	0.0	0.0	0	-9.1	0.0	0.0	0
<b>B-MB<sub>4</sub></b>	-9.4	0.0	0.0	0	-7.3	0.0	0.0	0
<b>I-MB<sub>1</sub></b>	-8.8	0.0	0.0	0	-8.6	0.0	0.0	0
<b>I-MB<sub>2</sub></b>	-10.6	0.0	0.0	0	-10.5	0.0	0.0	0
<b>I-MB<sub>3</sub></b>	-10.2	0.0	0.0	0	-8.1	0.0	0.0	0
<b>I-MB<sub>4</sub></b>	-9.4	0.0	0.0	0	-8.1	0.0	0.0	0
<b>Std. Isoniazid</b>	-7.2	0.0	0.0	0	-6	0.0	0.0	0

#### 4.2.1 Evaluation of outcomes

The produced test ligands' binding affinities against the TB gene targets PDB IDs 1ENY and 3R6C were assessed. With affinities ranging from -8.8 to -10.6 kcal/mol, all test compounds (B-MB1 to B-MB4 and I-MB1 to I-MB4) demonstrated noticeably greater binding to 1ENY than the common medication isoniazid. With the greatest affinity of -10.6 kcal/mol among

them, I-MB2 showed great promise as an inhibitor. All test compounds, with the exception of B-MB4, demonstrated superior binding to the 3R6C target compared to isoniazid. The binding affinities of I-MB1 to I-MB3 and B-MB1 to B-MB3 ranged from -8.1 to -10.5 kcal/mol. I-MB2 once more shown a strong affinity of -10.5 kcal/mol, confirming its possible effectiveness. Even though B-MB4's binding score was lower (-7.3 kcal/mol), it was still better than isoniazid. The majority of the test compounds, especially I-MB2, may be potential anti-TB medicines, according on the docking results overall.

### 4.3 Outcome of visualization

#### For Antifungal activity: PDB ID: 1U2J & 6F0E

Different interactions between a ligand and protein residues are depicted in the illustration. ARG B:668 and ARG B:691 form conventional hydrogen bonds. TRP B:653 has a pi-sulfur interaction, whereas SER B:686, LEU B:682, PHE B:663, and MET B:649 have pi-alkyl interactions. Furthermore, through van der Waals interactions, a number of residues, such as LEU B:646, GLY B:685, and others, support complex stability. (Fig.1)

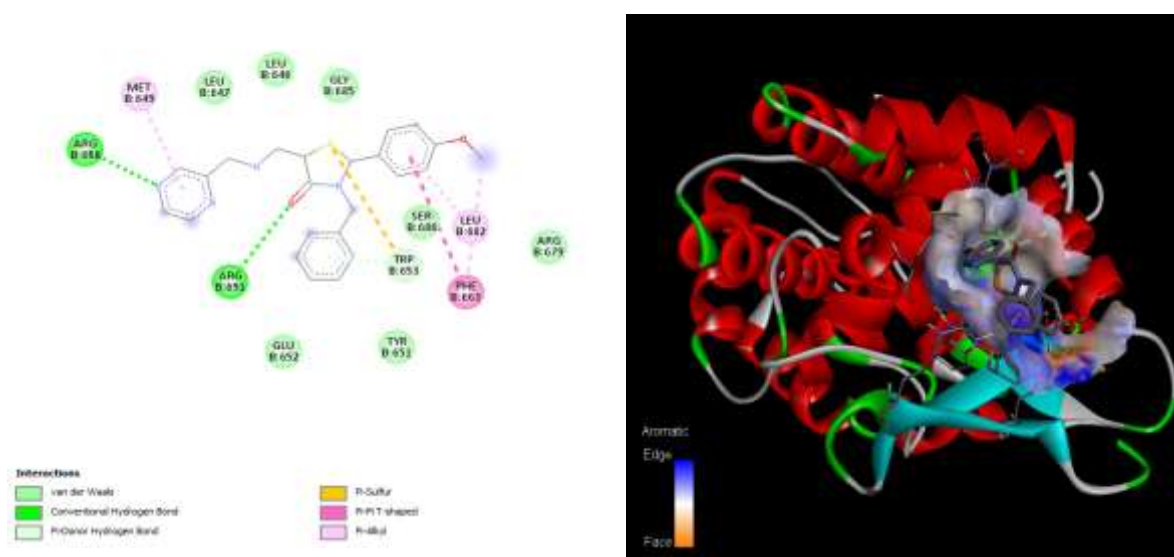


Fig. 1: 2D interaction & B-MB1 3D binding modes in active site (PDB ID: 1U2J)

The formation of conventional hydrogen bonds with ARG B:668 and ARG B:691 is essential for particular identification. Additionally important are pi-sulfur and pi-alkyl interactions, which involve residues like MET B:649, LEU B:682 and TRP B:653. Together, these particular bonds plus a large number of van der Waals interactions from nearby residues support the ligand's overall stability and strong binding inside the active site. (Fig.2)

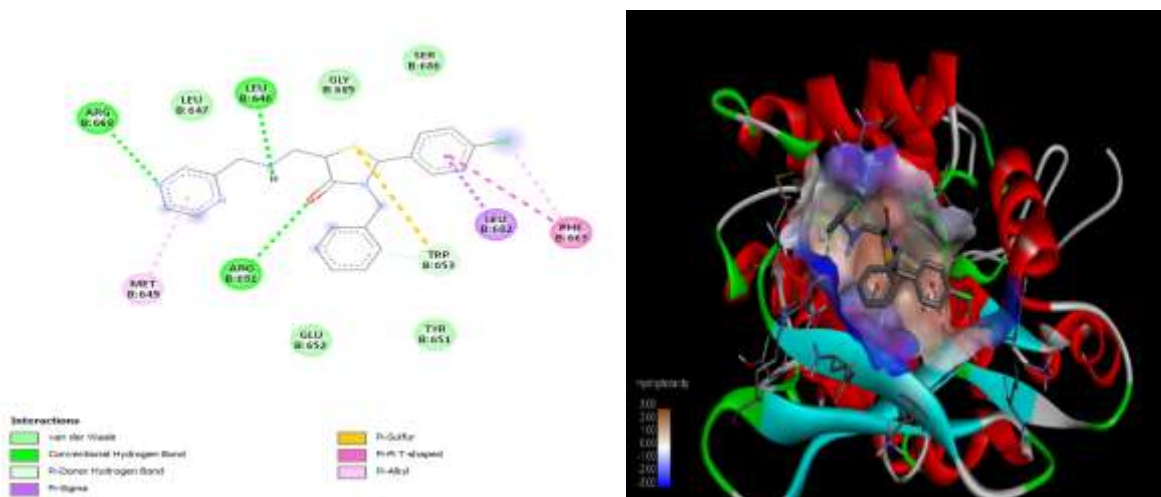


Fig. 2: 2D interaction & B-MB2 3D binding modes in active site (PDB ID: 1U2J)

The typical hydrogen bonds from ARG B:668 and ARG B:691 and describes the ligand-protein interactions that are essential for binding. Additional specialized interactions include pi-alkyl interactions with different residues such as LEU B:682 and MET B:649. TRP B:653 also has a pi-sulfur connection. Together, these many non-covalent forces and a large number of van der Waals interactions guarantee the ligand's stable binding. (Fig.3)

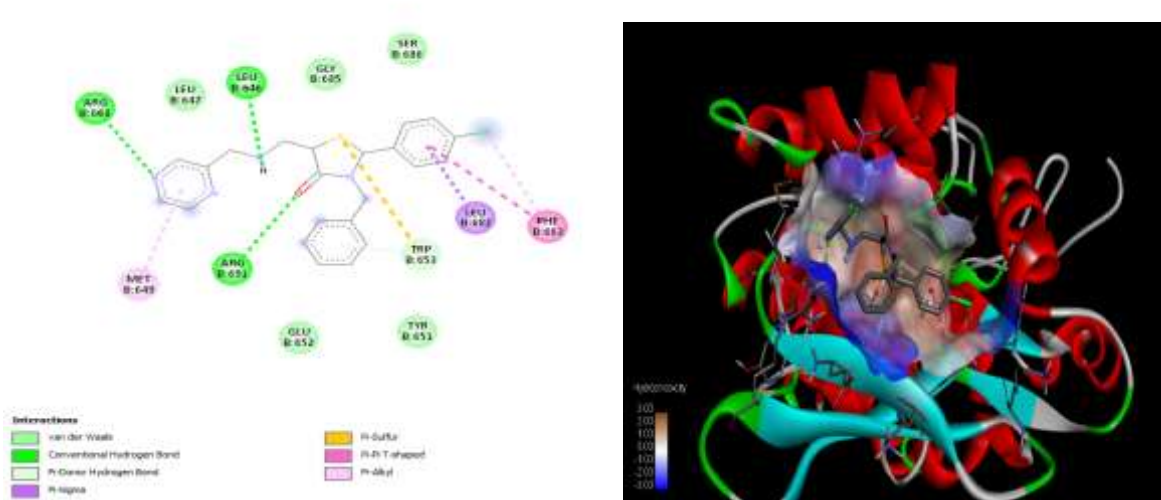


Fig. 3: 2D interaction & B-MB3 3D binding modes in active site (PDB ID: 1U2J)

Important ligand-protein interactions are depicted in the picture, such as the typical hydrogen bonds from ARG B:668 and ARG B:691. Additional particular interactions include pi-alkyl interactions with residues such as LEU B:682 and MET B:649. TRP B:653 also forms a pi-sulfur bond. Together, these many non-covalent forces and a large number of van der Waals interactions guarantee the ligand's stable binding. (Fig.4)

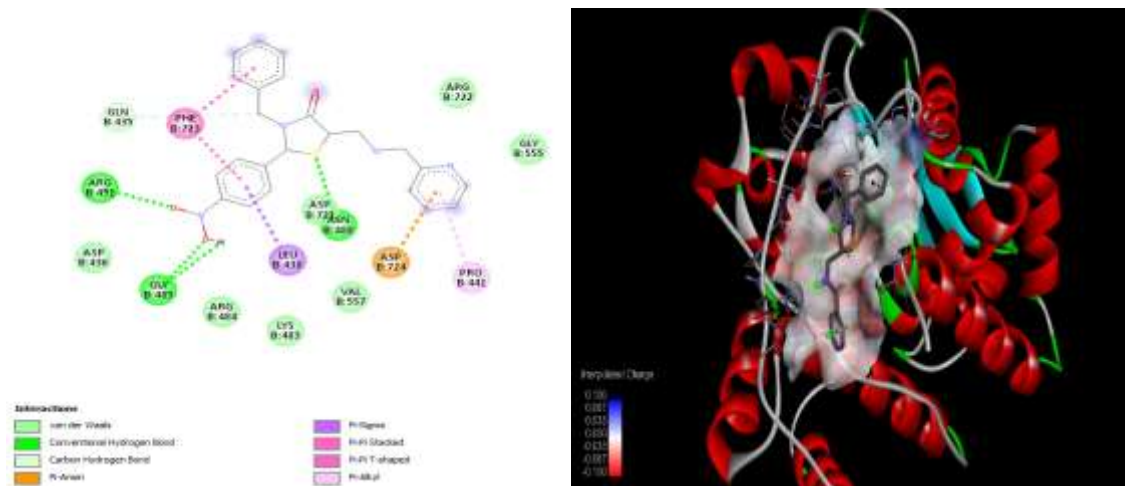


Fig.4: 2D interaction & B-MB4 3D binding modes in active site (PDB ID: 1U2J)

ARG B:

The complex is further stabilized by certain non-covalent contacts, such as a pi-sulfur bond from TRP B:653 and pi-alkyl interactions involving residues like LEU B:682 and MET B:649. Several van der Waals forces are mixed with these various interactions. (Fig.5)

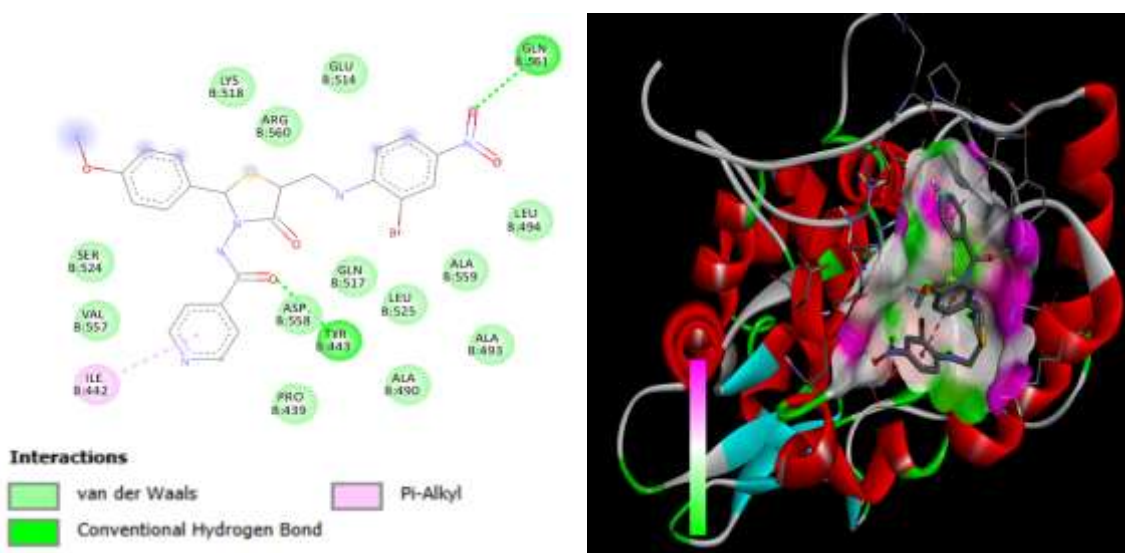


Fig. 5: 2D interaction & I-MB1 3D binding modes in active site (PDB ID: 1U2J)

Conventional hydrogen bonds between ASN B:719 and GLY B:481 and the ligand are important interactions. Pi-Alkyl interactions with residues such as LEU B:726, ALA B:553, and ILE B:442 are detected, indicating hydrophobic connections. Overall, the ligand's binding is stabilized by a combination of polar and hydrophobic forces, along with numerous van der Waals contacts with surrounding residues. (Fig.6)

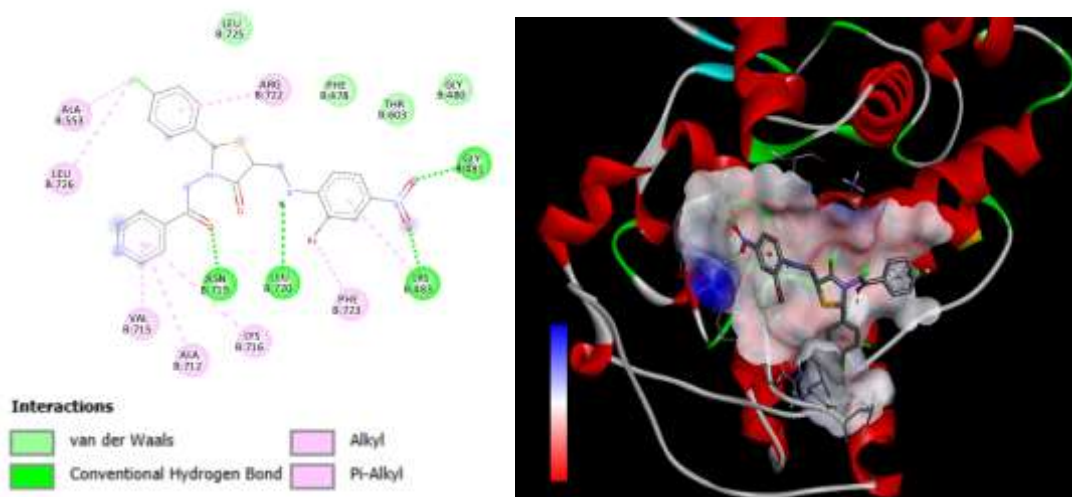


Figure 6: 2D interaction & I-MB2 3D binding modes in active site (PDB ID: 1U2J)

The picture shows how a ligand interacts with the amino acid residues of a protein's binding site. Along with Pi-Alkyl interactions with residues like ILE B:442 and PRO B:439, which indicate hydrophobic contacts, a crucial interaction is the traditional hydrogen bond between ARG B:560 and the ligand. With TYR B:443, pi-sigma interactions are also seen. Together with several van der Waals interactions, polar and hydrophobic forces stabilize the ligand's binding overall. (Fig.7)

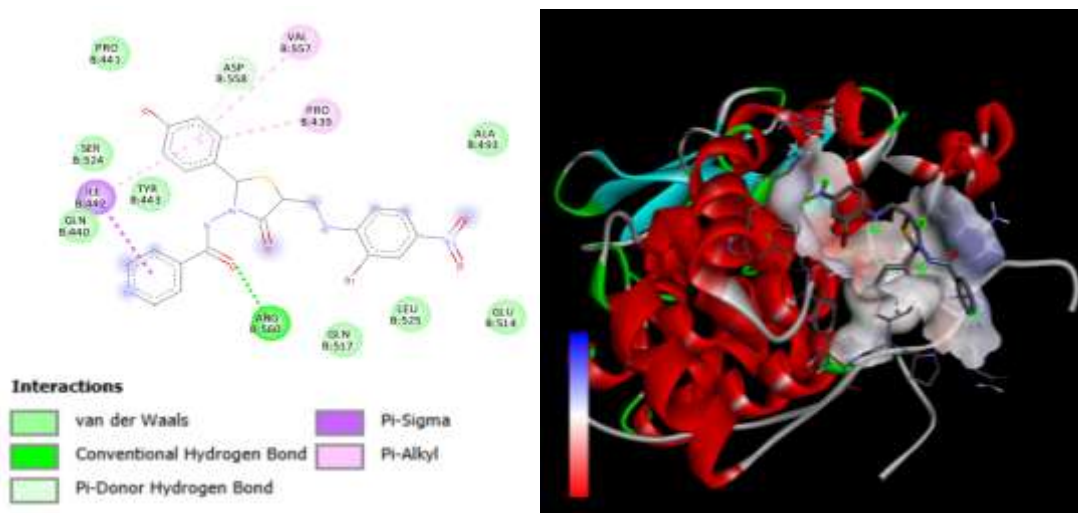


Figure 7: 2D interaction & I-MB3 3D binding modes in active site (PDB ID: 1U2J)

Conventional hydrogen bonds with the ligand that are produced by ASN B:719 and GLY B:481 are important interactions. Pi-Alkyl contacts are also formed by the ligand with VAL B:715, ALA B:712, and LEU B:726, Pi-Sigma interactions with LYS B:716, Pi-Pi T-shaped interactions with PHE B:723 and PHE B:478 and Amide-Pi Stacked interactions with ASN B:719 as well. Overall, polar and hydrophobic forces work together to stabilize the ligand's binding. (Fig.8)

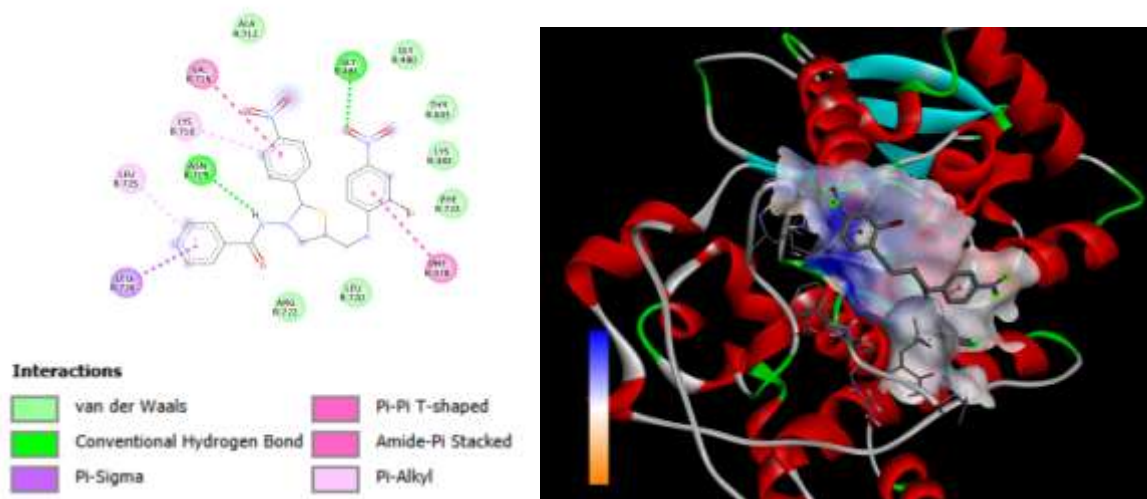


Figure 8 : 2D interaction & I-MB4 3D binding modes in active site (PDB ID: 1U2J)

The ligand and SER A:201 form a typical hydrogen bond, and TYR A:151 exhibits Pi-Pi T-shaped and Pi-Pi Stacked interactions, which suggest aromatic stacking. There are other hydrophobic interactions, such as Pi-Alkyl interactions with TYR A:111 and Alkyl contacts with VAL residues. Overall, a mix of hydrophobic, aromatic, and polar forces stabilizes the ligand's binding. (Fig.9)

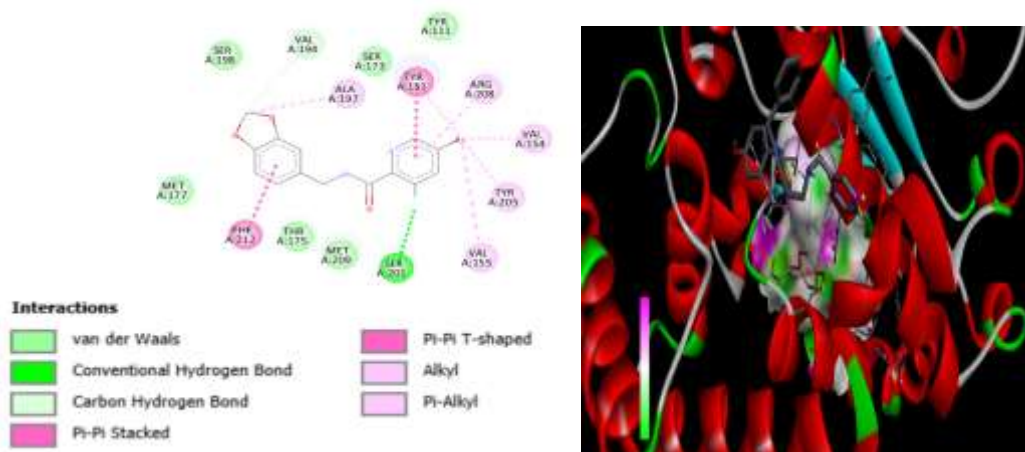


Fig. 9 : 2D interaction & B-MB1 3D binding modes in active site (PDB ID: 6F0E)

Two important interactions that show cation-aromatic and aromatic stacking, respectively, are the Pi-Cation interaction with ARG A:208 and the Pi-Pi Stacked interaction with PHE A:9. Alkyl and Pi-Alkyl interactions with LEU and TYR residues result in hydrophobic interactions. Together with van der Waals forces and carbon hydrogen bonds, these interactions stabilize the ligand's binding overall. (Fig.10)

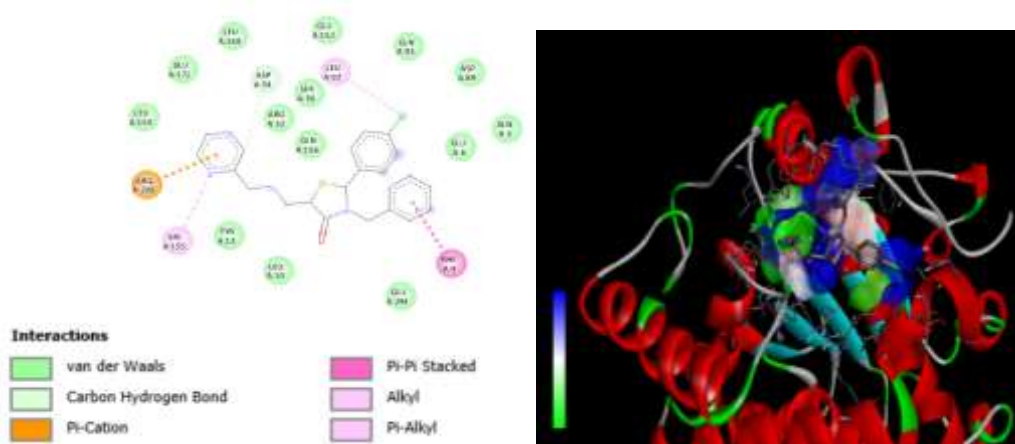


Fig. 10: 2D interaction & B-MB2 3D binding modes in active site (PDB ID: 6F0E)

Pi-Anion interactions with GLU A:6, traditional hydrogen bonds with ARG A:52 and THR A:97, and Pi-Pi Stacked interactions with PHE A:9 are important interactions. Pi-Alkyl interactions with residues such as VAL A:155 and LEU A:53 result in hydrophobic contacts. Overall, a mix of hydrophobic, hydrogen bonding, aromatic stacking, and electrostatic forces stabilizes the ligand's binding. (Fig.11)

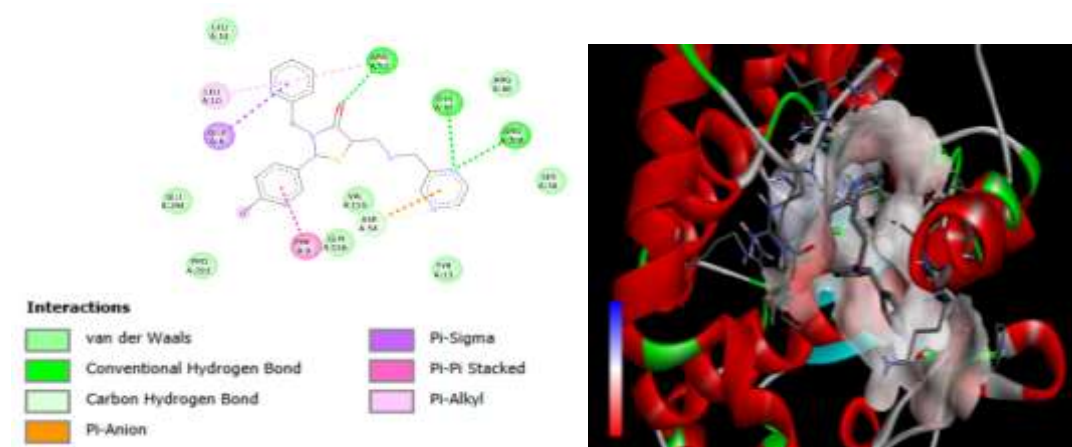


Fig. 11 : 2D interaction & B-MB3 3D binding modes in active site (PDB ID: 6F0E)

Pi-Cation interactions with ARG A:208, Pi-Sigma interactions with ARG A:52, and Pi-Pi T-shaped interactions with PHE A:9 are important interactions that show cation-aromatic and aromatic stacking. Through Alkyl and Pi-Alkyl connections involving VAL A:155, TYR A:13, and LEU A:159, hydrophobic interactions are present. Together with van der Waals forces and hydrogen bonds, these interactions stabilize the ligand's binding overall. (Fig.12)

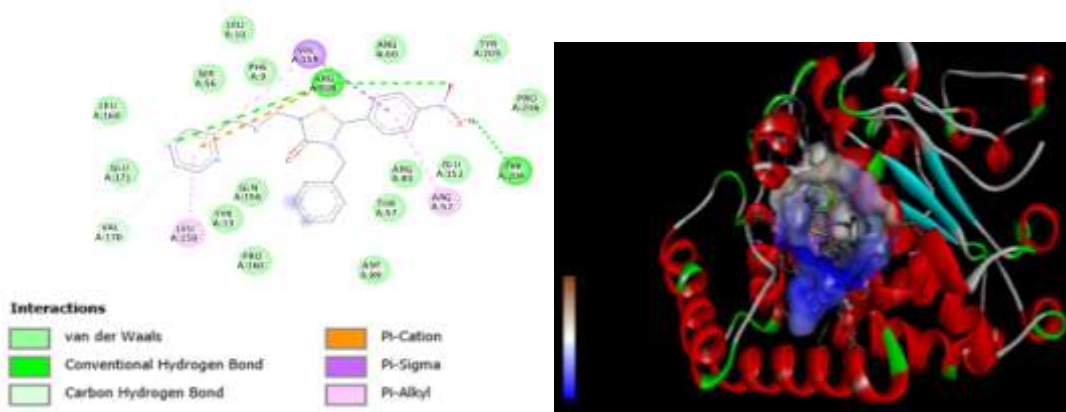


Fig. 12 : 2D interaction & B-MB4 3D binding modes in active site (PDB ID: 6F0E)

The Pi-Pi T-shaped contact with PHE A:9, which indicates aromatic stacking, and the traditional hydrogen bonds that ARG A:208 and SER A:56 create with the ligand. Pi-Alkyl interactions with residues such as TYR A:13, LEU A:92, and VAL A:155 result in hydrophobic contacts. Overall, a mix of hydrophobic and polar forces stabilizes the ligand's binding. (Fig.13)

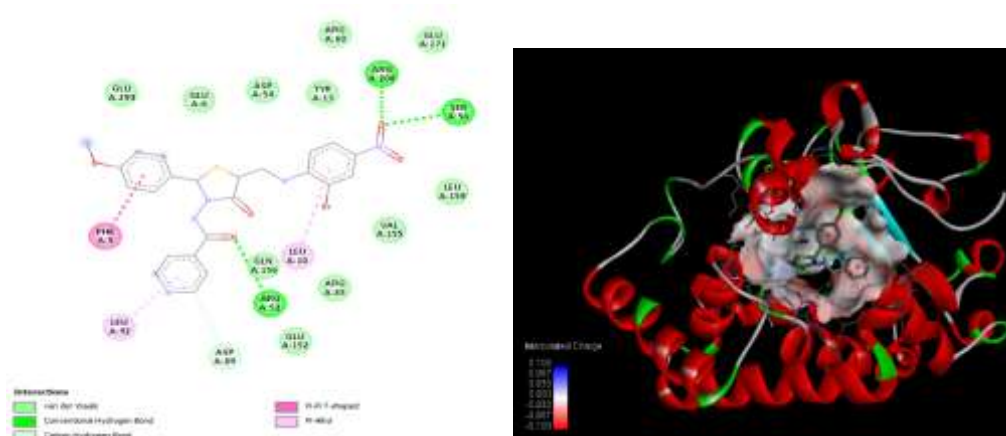


Fig. 13: 2D interaction & I-MB1 3D binding modes in active site (PDB ID: 6F0E)

Important interactions include the Pi-Pi Stacked interaction with PHE A:9, which indicates aromatic stacking, and the traditional hydrogen bonds that ARG A:208 and TYR A:205 make with the ligand. Alkyl and Pi-Alkyl interactions with residues such as VAL A:155, TYR A:13, and LEU A:92 result in hydrophobic contacts. Overall, a mix of hydrophobic and polar forces stabilizes the ligand's binding. (Fig.14)

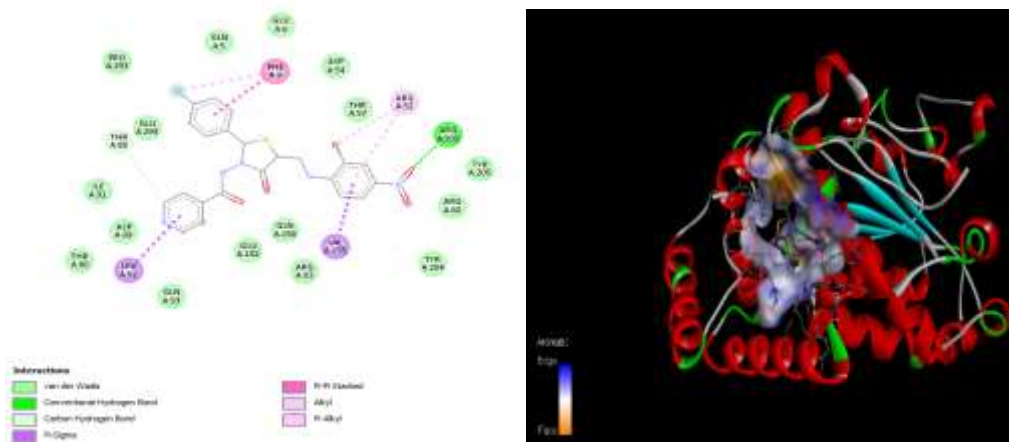
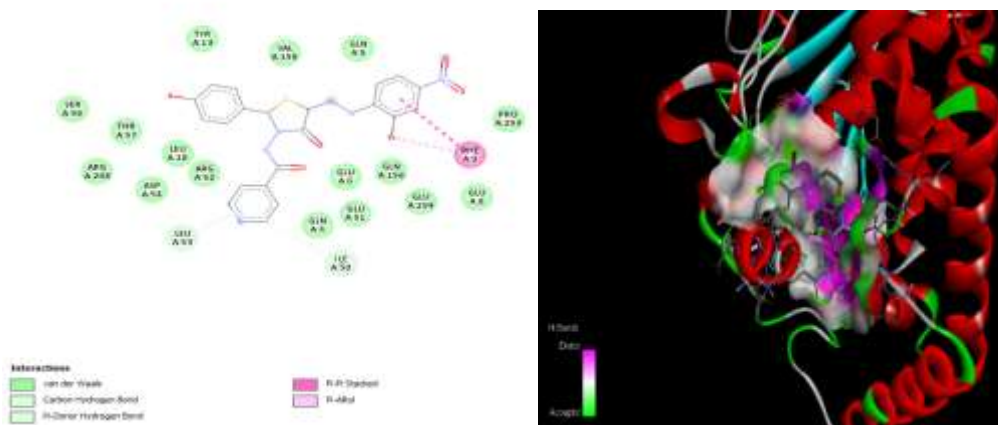


Fig. 14: 2D interaction & I-MB2 3D binding modes in active site (PDB ID: 6F0E)

The picture shows how a ligand interacts with the amino acid residues of a protein's binding site. Pi-Pi Stacked interactions with PHE A:9, which show aromatic stacking, and a Pi-Donor Hydrogen Bond from GLN A:5 are important interactions. Alkyl and Pi-Alkyl contacts involving VAL A:155, TYR A:13, and LEU residues result in hydrophobic interactions. Overall, a mix of hydrophobic and polar forces stabilizes the ligand's binding. (Fig.15)



Crucial interact: Fig. 15: 2D interaction & I-MB3 3D binding modes in active site (PDB ID: 6F0E)

Crucial interact: bonds that TYR A:205 and ARG A:208 establish with the ligand. Pi-Pi Stacked interactions with PHE A:9 result in aromatic stacking. Alkyl and Pi-Alkyl interactions with residues such as VAL A:155 and TYR A:157 result in hydrophobic contacts. (Fig.16)

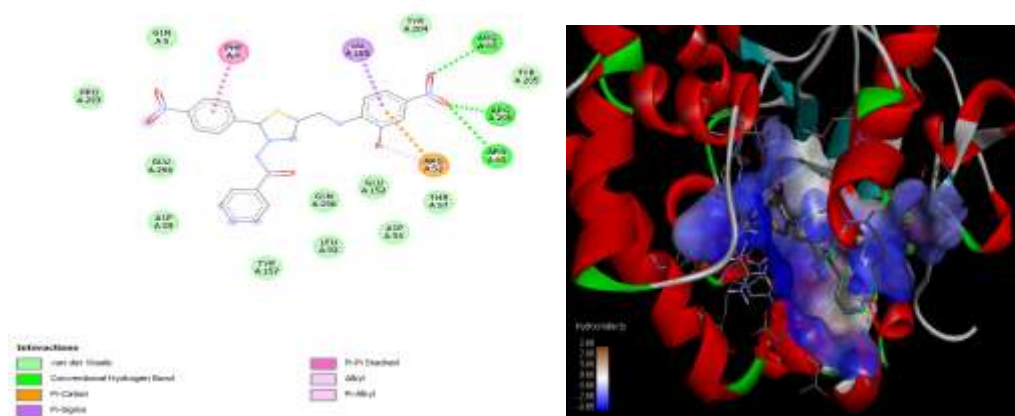


Fig. 16: 2D interaction & I-MB4 3D binding modes in active site (PDB ID: 6F0E)

**For Antitubercular activity: PDB ID: 1ENY & PDB ID: 3R6C**

Notable interactions include Pi-Pi Stacked interactions with PHE A:97, which show aromatic stacking, and conventional hydrogen bonds made with the ligand between SER A:94 and GLY A:96. Alkyl and Pi-Alkyl interactions involving ILE residues result in hydrophobic interactions. Overall, a mix of hydrophobic and polar forces stabilizes the ligands. (Fig.17)

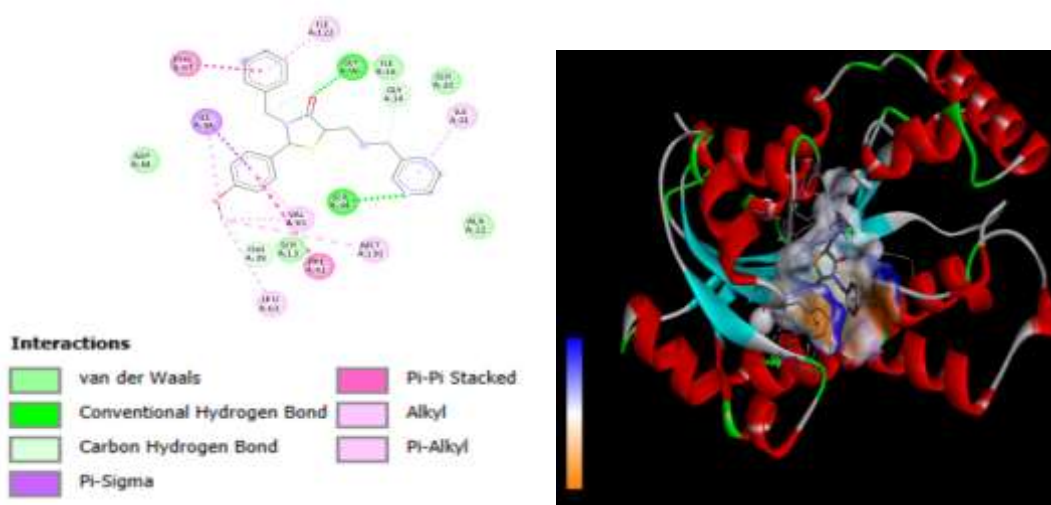


Fig. 17: 2D interaction & B-MB1 3D binding modes in active site (PDB ID: 1ENY)

The picture demonstrates the way amino acid residues in a protein's binding site interact with a ligand. Pi-Pi Stacked interactions with PHE A:97, which show aromatic stacking, and traditional hydrogen bonds made between SER A:94 and GLY A:96 and the ligand are important interactions. Through Alkyl and Pi-Alkyl interactions involving ILE residues, hydrophobic interactions exist. Overall, polar and hydrophobic forces work together to stabilize the ligand's binding. (Fig.18)

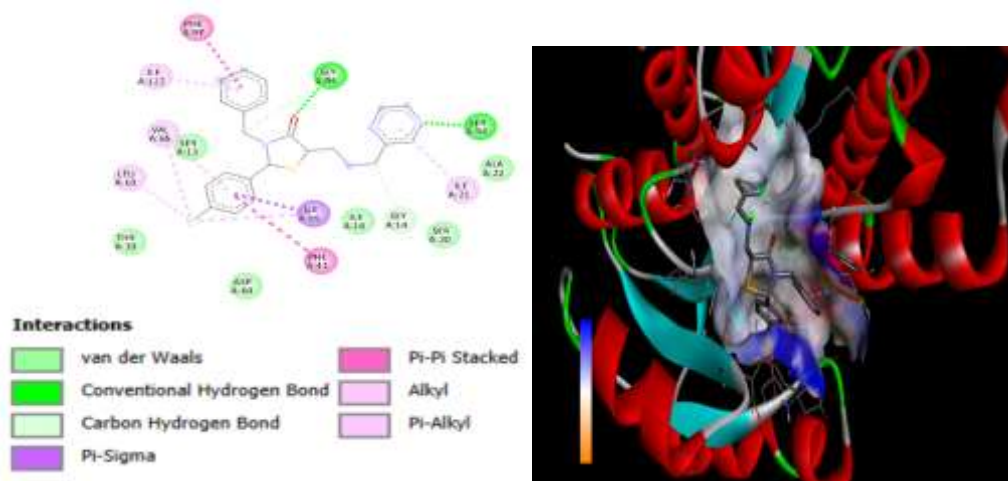


Fig. 18: 2D interaction & B-MB2 3D binding modes in active site (PDB ID: 1ENY)

Pi-Pi Stacked interactions with PHE A:97 and Pi-Pi T-shaped contacts with PHE A:41, which indicate aromatic stacking, are important interactions, as are the traditional hydrogen bonds that are generated between SER A:96 and THR A:196 with the ligand. Alkyl and Pi-Alkyl contacts involving ILE residues and VAL A:65 result in hydrophobic interactions. Overall, a mix of hydrophobic and polar forces stabilizes the ligand's binding. (Fig.19)

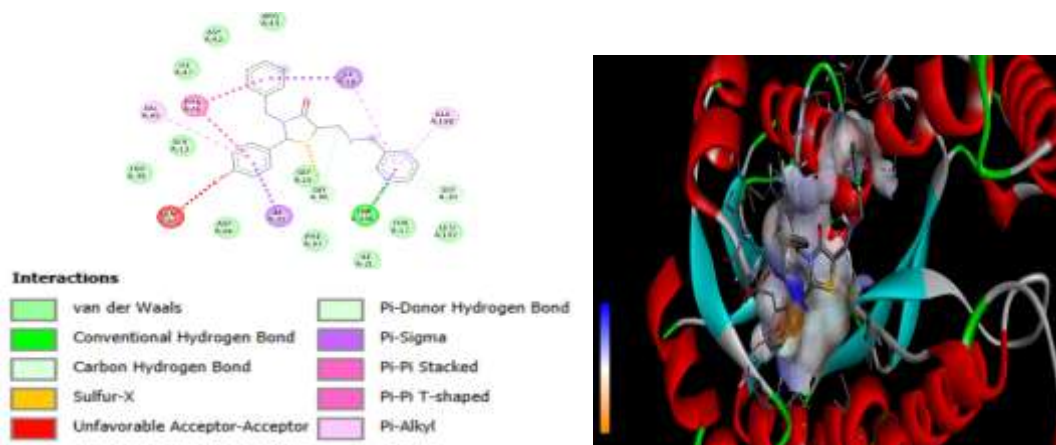


Fig. 19: 2D interaction & B-MB3 3D binding modes in active site (PDB ID: 1ENY)

Key interactions include Pi-Pi Stacked interactions with PHE A:97, indicating aromatic stacking, and conventional hydrogen bonds made with the ligand between SER A:94 and GLY A:96. Alkyl and Pi-Alkyl contacts involving ILE residues and VAL A:65 result in hydrophobic interactions. The ligand exhibits a Pi-Sulfur interaction with MET A:147. (Fig.20)

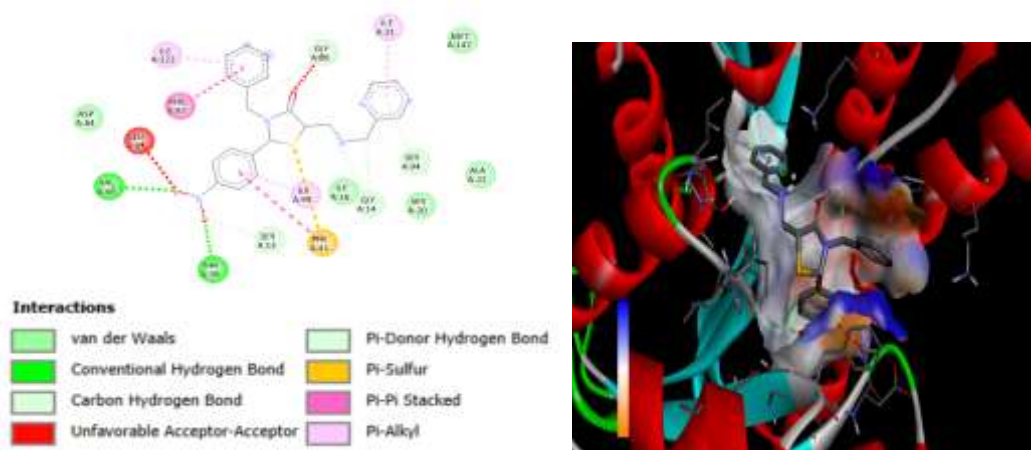


Fig. 20: 2D interaction & B-MB4 3D binding modes in active site (PDB ID: 1ENY)  
 The picture shows how a ligand interacts with the amino acid residues of a protein's binding site. Important interactions include Pi-Pi Stacked interactions with PHE A:97, which show aromatic stacking, and conventional hydrogen bonds made with the ligand between SER A:94 and GLY A:96. Alkyl and Pi-Alkyl contacts involving ILE residues and VAL A:65 result in hydrophobic interactions. The ligand and THR A:39 create a Pi-Donor Hydrogen Bond. (Fig.21)

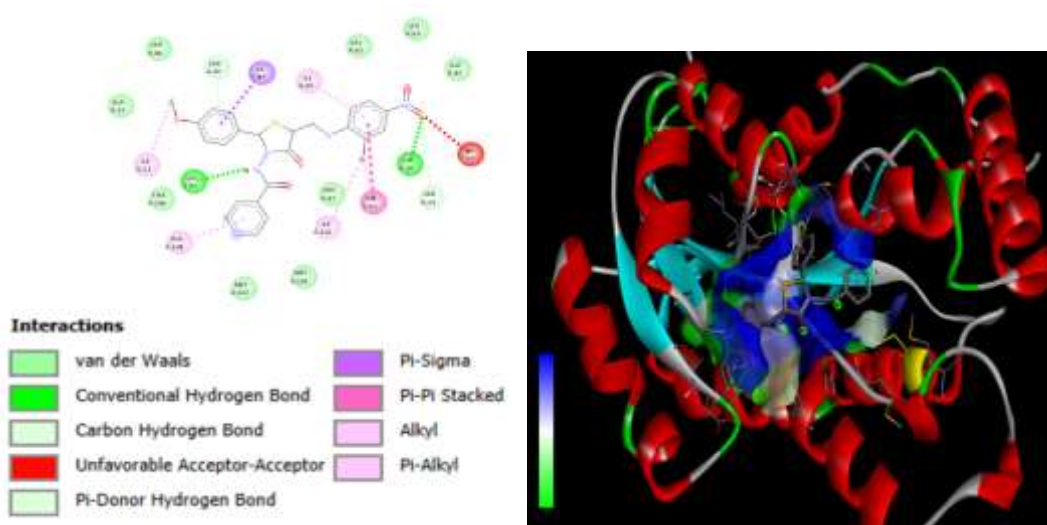


Fig. 21: 2D interaction & I-MB1 3D binding modes in active site (PDB ID: 1ENY)

The image illustrates the interactions that take place at the binding site of a protein between a ligand and amino acid residues. Important interactions include Pi-Pi Stacked interactions with PHE A:97, which show aromatic stacking, and conventional hydrogen bonds made with the ligand between SER A:94 and GLY A:96. Alkyl and Pi-Alkyl contacts involving ILE residues and VAL A:65 result in hydrophobic interactions. The ligand and THR A:39 create a Pi-Donor Hydrogen Bond. (Fig.22)

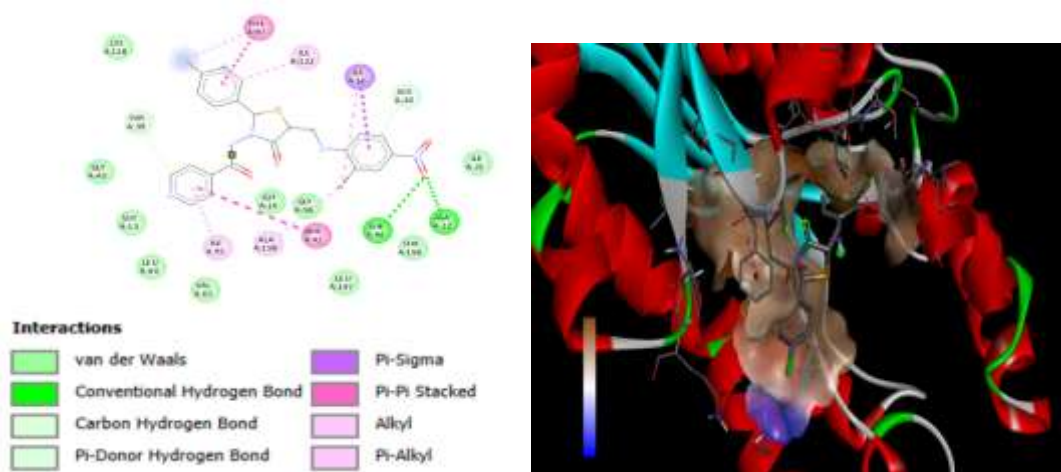


Fig. 22: 2D interaction & I-MB2 3D binding modes in active site (PDB ID: 1ENY)

The vital binding forces that hold the ligand and protein together. Pi-Pi Stacked contacts with PHE A:97 and PHE A:41 are notable interactions that indicate significant aromatic stacking. Numerous ILE, VAL, and LEU residues exhibit hydrophobic interactions, including Alkyl and Pi-Alkyl. Furthermore, a Pi-Sigma interaction with ASP A:64 and several van der Waals forces work together to support the ligand's stable binding in the active site. (Fig.23)

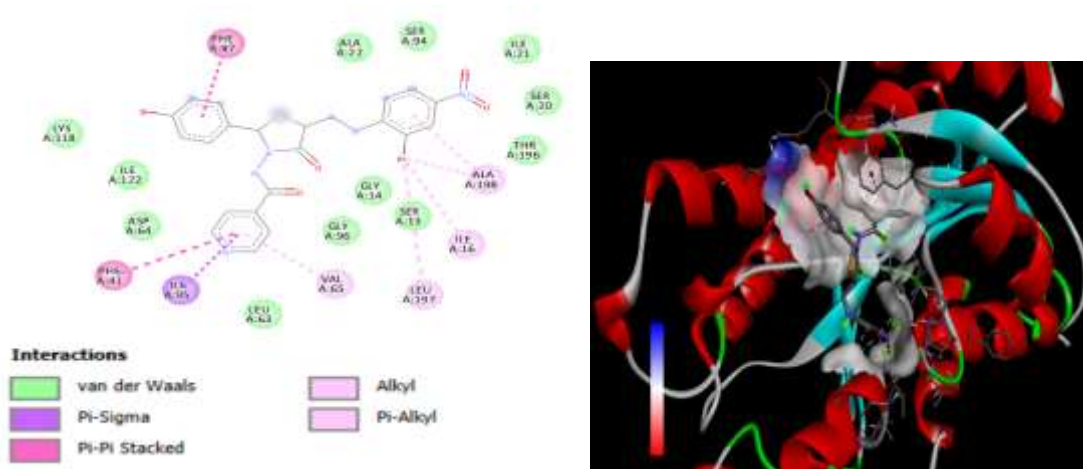


Fig. 23: 2D interaction & I-MB3 3D binding modes in active site (PDB ID: 1ENY)

It forms important conventional hydrogen bonds with ALA A:22, SER A:94, and GLY A:14. Pi-Alkyl interactions including ILE A:16, ILE A:95, and ALA A:198 clearly show hydrophobic contacts. Several van der Waals forces from nearby residues contribute to the total binding, and an unfavorable acceptor-acceptor interaction is seen with THR A:39. (Fig.24)

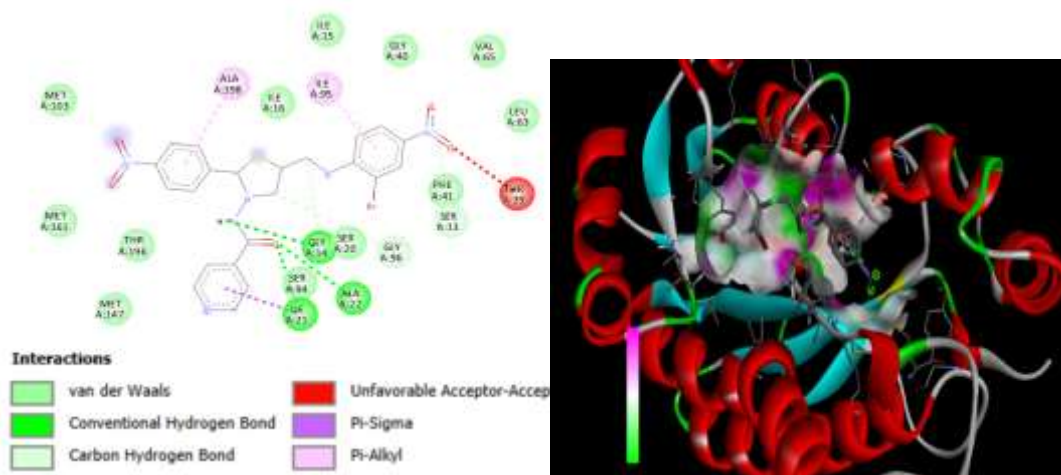


Fig. 24: 2D interaction & I-MB4 3D binding modes in active site (PDB ID: 1ENY)

SER B:143 and ASN B:138, hydrogen bonds are created. ARG B:193 has a notable Pi-Cation interaction. Alkyl interactions with ALA B:179 demonstrate hydrophobic contacts, and the ligand-protein complex is further stabilized by a variety of van der Waals forces from nearby residues, including SER B:142, ARG B:139, and GLY B:206. (Fig.25)

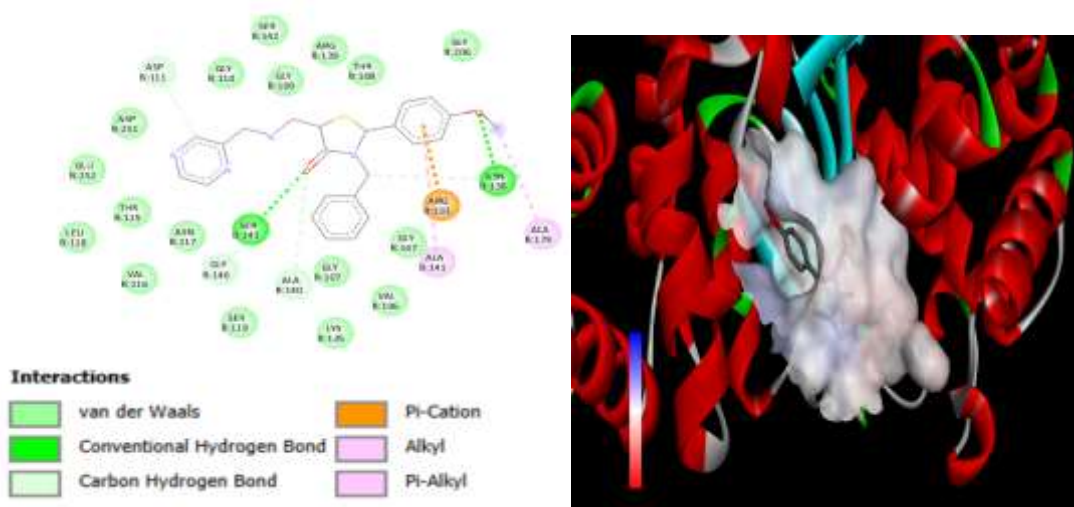


Fig. 25: 2D interaction & B-MB1 3D binding modes in active site (PDB ID: 6F0E)

GLY B:109, ALA B:140, and THR B:108 all create hydrogen bonds. Hydrophobic contacts are indicated by the presence of Pi-Alkyl interactions with VAL B:106, GLY B:137, and ALA B:179, as well as Amide-Pi Stacked interactions with GLY B:206. Several van der Waals forces from nearby residues, including ASP B:251 and GLU B:252, also support the ligand-protein complex's overall stability. (Fig.26)

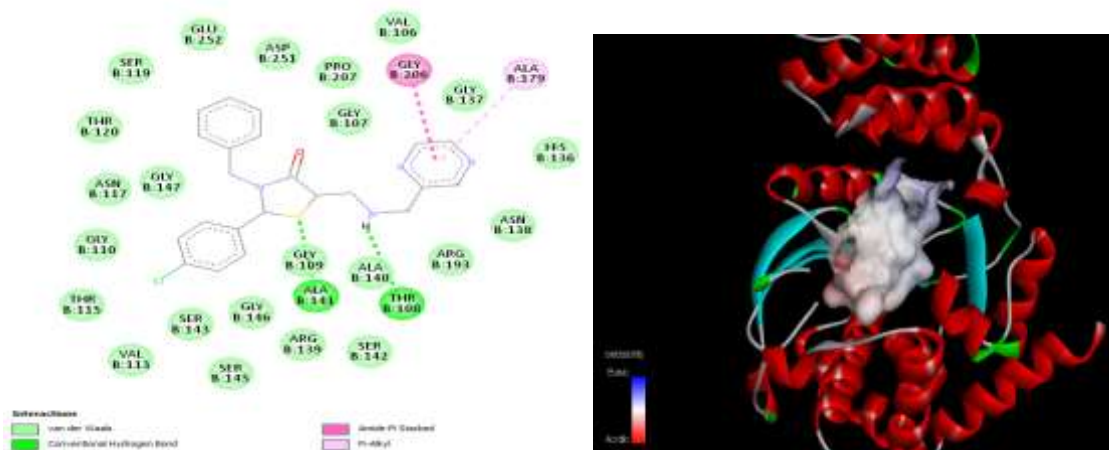


Fig. 26: 2D interaction & B-MB2 3D binding modes in active site (PDB ID: 6F0E)

Substantial conventional hydrogen bonds are established with ASN B:138 and GLY B:109. Hydrophobic contacts are indicated by the presence of Pi-Alkyl interactions with VAL B:106, GLY B:137, and ALA B:179, as well as Amide-Pi Stacked interactions with GLY B:206. Interestingly, there is an unfavorable donor-donor contact with GLU B:252 and an unfavorable acceptor-acceptor interaction with ARG B:193, which may indicate areas for improvement. (Fig.27)

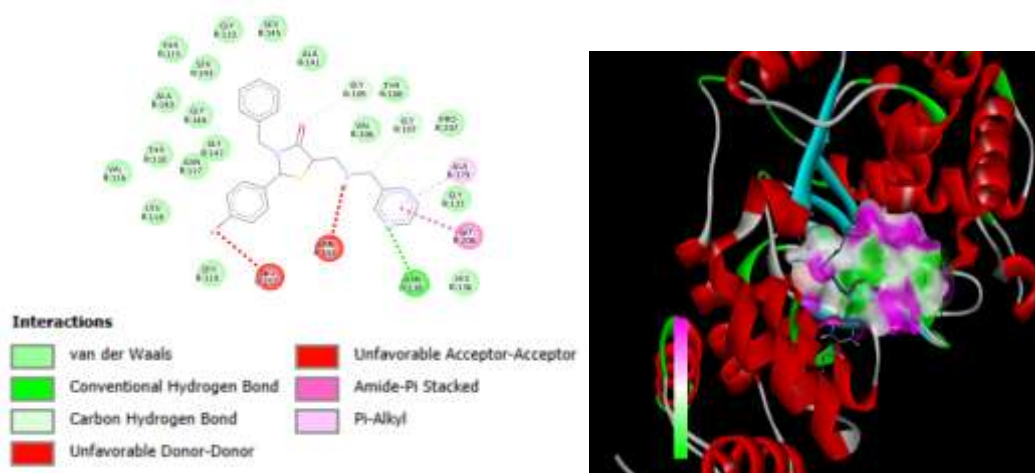


Fig. 27: 2D interaction & B-MB3 3D binding modes in active site (PDB ID: 6F0E)

Several typical hydrogen bonds are shown in this picture, which depicts the two-dimensional interactions between a ligand and protein residues. Important anchor points are provided by interactions with THR B:108, GLY B:110, ASN B:138, SER B:143, GLY B:109, SER B:119, and GLU B:252. LYS B:135 and GLY B:147 exhibit carbon hydrogen bonding. Furthermore, a large number of van der Waals forces from nearby residues support the ligand-protein complex's overall stability. (Fig.28)

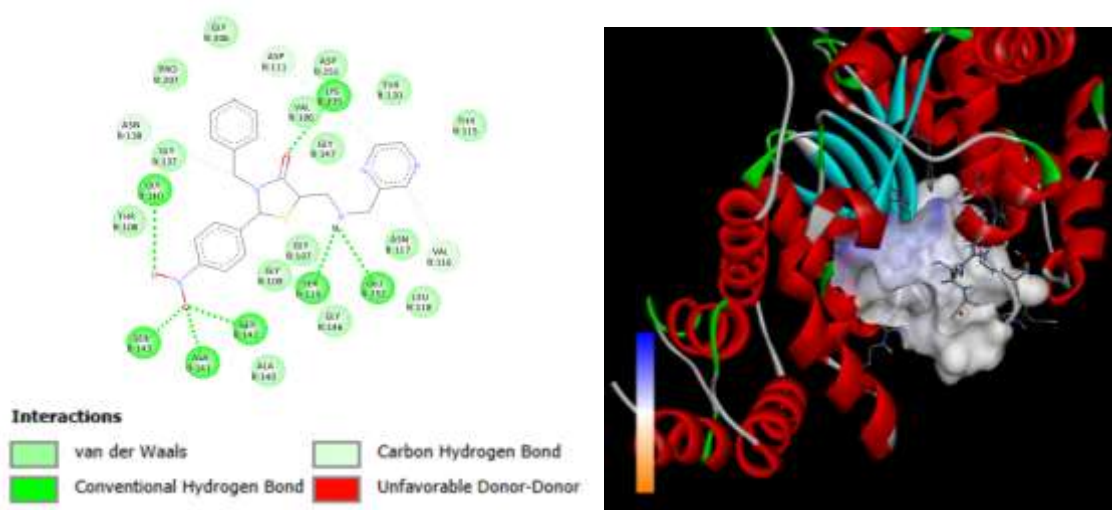


Fig. 28: 2D interaction & B-MB4 3D binding modes in active site (PDB ID: 6F0E)

A conventional hydrogen bond is formed with ASN B:138, and a Pi-Cation interaction is observed with ARG B:193, indicating an electrostatic interaction. Pi-Pi T-shaped interactions are present with PHE B:178, signifying aromatic stacking. Additionally, Pi-Alkyl interactions with ALA B:190 and ARG B:187, along with Carbon Hydrogen Bonds with PRO B:180 and PRO B:207, contribute to the overall stability of the ligand-protein complex. (Fig.29)

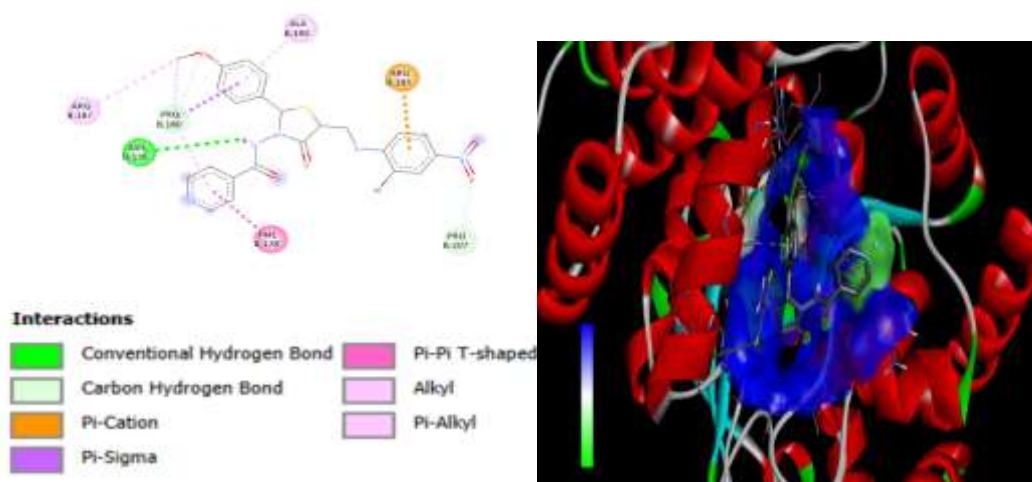


Fig. 29: 2D interaction & I-MB1 3D binding modes in active site (PDB ID: 6F0E)

Key conventional hydrogen bonds are formed with GLY B:107, ARG B:193, and THR B:120, providing critical anchor points. Hydrophobic interactions are also prominent, with Alkyl interactions involving VAL B:106 and Pi-Alkyl interactions with TYR B:186 and LEU B:205. Additionally, a Pi-Donor Hydrogen Bond is observed with SER B:119, and Carbon Hydrogen Bonds are present with LEU B:118 and GLY B:137, all contributing to the overall stability and specificity of the ligand-protein complex. (Fig.30)

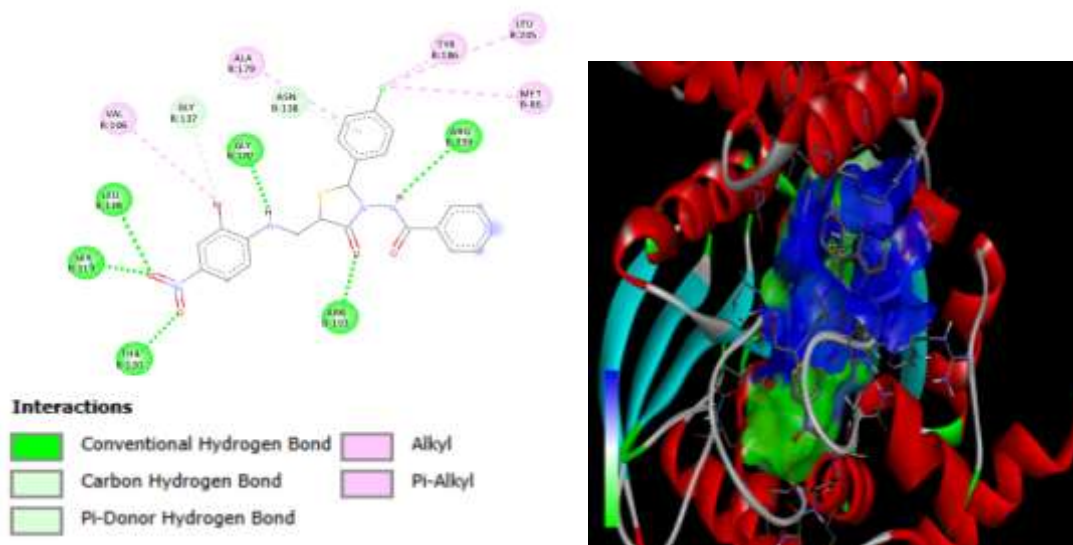


Fig. 30: 2D interaction & I-MB2 3D binding modes in active site (PDB ID: 6F0E)

Crucial anchor sites are provided by the formation of important conventional hydrogen bonds with ASN B:138 and ARG B:194. Favorable aromatic interactions are shown by the Amide-Pi Stacked interactions with ALA B:190 and ALA B:179. The complex's hydrophobic stability is further influenced by Pi-Alkyl interactions with ALA B:140, ALA B:141, and PRO B:180. (Fig.31)

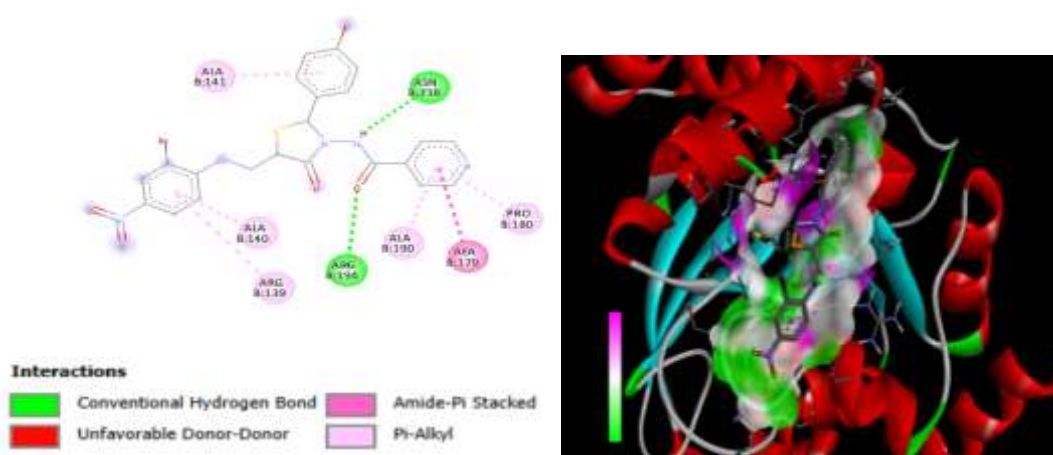


Fig. 31: 2D interaction & I-MB3 3D binding modes in active site (PDB ID: 6F0E)

ARG B:139, ARG B:194, and GLY B:206 create important conventional hydrogen bonds that serve as vital anchor points. With ARG B:193, a notable Pi-Cation interaction is seen. The hydrophobic stability of the complex is further enhanced by Pi-Alkyl interactions with PRO B:180, ARG B:187, and ALA B:141, as well as a Halogen bond with bromine. (Fig.32)

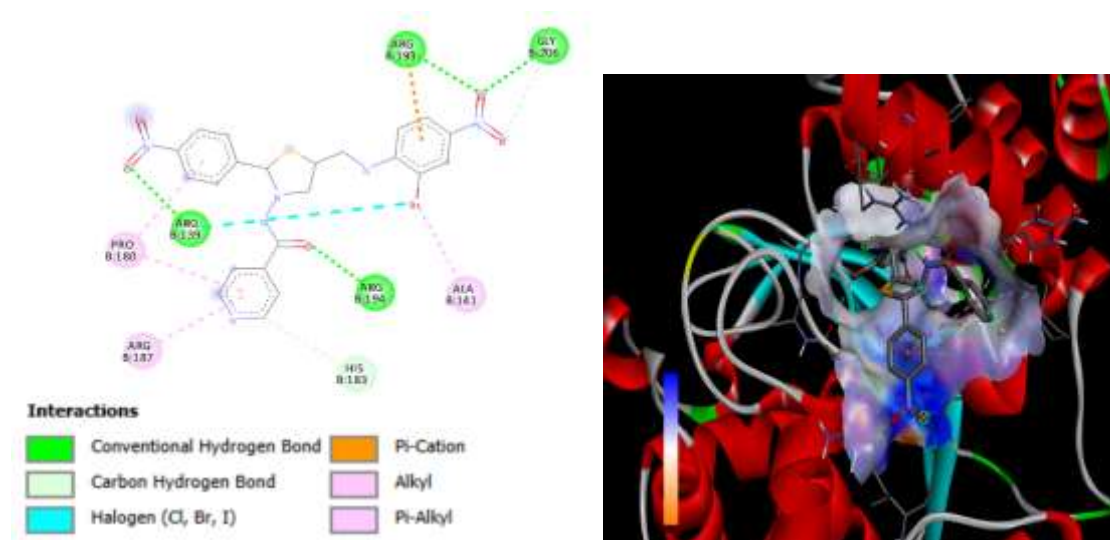


Fig. 32: 2D interaction & I-MB4 3D binding modes in active site (PDB ID: 6F0E)

## 5. Discussion

The present study demonstrated the potential of newly synthesized heterocyclic compounds as dual-action antifungal and antitubercular agents using molecular docking techniques. Among the compounds screened, I-MB2 exhibited the highest binding affinities of  $-10.4$  kcal/mol (Sec14p, 6F0E) and  $-10.6$  kcal/mol (InhA, 1ENY), outperforming standard drugs like fluconazole and isoniazid. This suggests that I-MB2 has a strong potential to inhibit both fungal and mycobacterial targets effectively. Compounds B-MB3 and I-MB3 also showed promising multi-target interactions, indicating a favorable structural framework for broad-spectrum activity. The docking studies highlighted key interactions such as hydrogen bonding and hydrophobic contacts that contribute to ligand stability within the active sites. These findings reinforce the role of rational drug design in identifying effective antimicrobial scaffolds. However, molecular docking provides only predictive insights, and further experimental validation is essential. Future studies should include *in vitro* and *in vivo* evaluations to confirm the biological activity and safety profiles of these compounds. Overall, the results support the potential of heterocyclic derivatives—particularly I-MB2—as strong candidates for developing new antimicrobial therapies.

## 6. Conclusion

This study identified novel heterocyclic compounds with significant antifungal and antitubercular potential using molecular docking. Among them, I-MB2 showed the strongest binding affinities, outperforming standard drugs like fluconazole and isoniazid. Compounds B-MB3 and I-MB3 also exhibited promising multi-target activity. The docking results suggest these compounds interact effectively with key microbial proteins, indicating strong therapeutic potential. While the *in silico* results are encouraging, further experimental validation is necessary. Overall, the findings support the potential of these compounds, especially I-MB2, as candidates for developing dual-action antimicrobial agents.

## 7. References

1. [1] World Health Organization. *Global tuberculosis report 2023*. <https://www.who.int/tb>
2. Pai M, Behr MA, Dowdy D, Dheda K, Divangahi M, Boehme CC, Ginsberg A, Swaminathan S, Spigelman M, Getahun H. *Nature reviews disease primers. Tuberculosis*. 2016;2(16076):10-38.
3. Sharma SK, Mohan A. *Multidrug-resistant tuberculosis. Indian Journal of Medical Research*. 2004;120(4):354-76.
4. Sankineni S, Chauhan S, Shegokar R, Pathak Y. *Global health and tuberculosis; past, present, and future. In Tubercular Drug Delivery Systems: Advances in Treatment of Infectious Diseases 2023 Mar 15 (pp. 1-13). Cham: Springer International Publishing*.
5. Bongomin F, Gago S, Oladele RO, Denning DW. *Global and multi-national prevalence of fungal diseases—estimate precision. Journal of fungi*. 2017 Oct 18;3(4):57.
6. Brown GD, Denning DW, Gow NA, Levitz SM, Netea MG, White TC. *Hidden killers: human fungal infections. Sci Transl Med 4: 165rv13 [Internet]. 2012*
7. Denning DW, Pleuvry A, Cole DC. *Global burden of allergic bronchopulmonary aspergillosis with asthma and its complication chronic pulmonary aspergillosis in adults. Medical mycology*. 2013 May 1;51(4):361-70.
8. Zumla A, et al. *Drug-resistant tuberculosis—current dilemmas. N Engl J Med*. 2013;368(23):2192–2200.
9. Kaur G, Chawla S, Kumar P, Singh R. *Advancing vaccine strategies against Candida infections: exploring new frontiers. Vaccines*. 2023 Oct 29;11(11):1658.
10. Arastehfar A, Gabaldón T, Garcia-Rubio R, Jenks JD, Hoenigl M, Salzer HJ, Ilkit M, Lass-Flörl C, Perlin DS. *Drug-resistant fungi: an emerging challenge threatening our limited antifungal armamentarium. Antibiotics*. 2020 Dec 8;9(12):877.
11. Pontali E, et al. *MDR/XDR-TB treatment: drug development and clinical strategies. J Antimicrob Chemother*. 2017;72(5):1363–1374.
12. Tiberi S, Utjesanovic N, Galvin J, Centis R, D'Ambrosio L, van den Boom M, Zumla A, Migliori GB. *Drug resistant TB—latest developments in epidemiology, diagnostics and management. International Journal of Infectious Diseases*. 2022 Nov 1;124:S20-5.
13. Walker J, Edwards WS, Hall NM, Pappas PG. *Challenges in management of invasive fungal infections in stem cell transplant. Transplant Infectious Disease*. 2023 Nov;25:e14175.
14. Cowen LE, Steinbach WJ. *Stress, drugs, and evolution: the role of cellular signaling in fungal drug resistance. Eukaryotic cell*. 2008 May;7(5):747-64.
15. Joule JA. *Heterocyclic chemistry. CRC Press; 2020 Nov 25*.
16. Hung TQ, Dang TT, Pham NN, Langer P. *SYNTHESIS OF FUSED AROMATIC N-HETEROCYCLES BY DOMINO SITE-SELECTIVE PALLADIUM-CATALYZED CC AND CN COUPLING REACTIONS. Targets in Heterocyclic Systems Chemistry and Properties*. 2017;21:389-401.
17. Mao F, Ni W, Xu X, Wang H, Wang J, Ji M, Li J. *Chemical structure-related drug-like criteria of global approved drugs. Molecules*. 2016 Jan 12;21(1):75.
18. Keri RS, Patil MR, Patil SA, Budagumpi S. *A comprehensive review in current developments of benzothiazole-based molecules in medicinal chemistry. European Journal of Medicinal Chemistry*. 2015 Jan 7;89:207-51.

19. Albain KS, Barlow WE, Shak S. *Bibliography Current World Literature Vol 22 No 6 November 2010. Ann Oncol. 2010;21:238-44.*
20. Sharma AS, Salahuddin, Mazumder A, Kumar R, Datt V, Shabana K, Tyagi S, Shahar Yar M, Jawed Ahsan M. *Recent updates on synthesis, biological activity, and structure-activity relationship of 1, 3, 4-oxadiazole-quinoline hybrids: a review. Current Organic Synthesis. 2023 Nov 1;20(7):758-87.*
21. Samala G, Kakan SS, Nallangi R, Devi PB, Sridevi JP, Saxena S, Yogeewari P, Sriram D. *Investigating structure–activity relationship and mechanism of action of antitubercular 1-(4-chlorophenyl)-4-(4-hydroxy-3-methoxy-5-nitrobenzylidene) pyrazolidine-3, 5-dione [CD59]. International Journal of Mycobacteriology. 2014 Jun 1;3(2):117-26.*
22. Chuprun SS, Kantin G, Krasavin M. *Synthesis and medicinal applications of N-aryl-C-nitroazoles. Mini Reviews in Medicinal Chemistry. 2018 Dec 1;18(20):1733-52.*
23. Meng XY, Zhang HX, Mezei M, Cui M. *Molecular docking: a powerful approach for structure-based drug discovery. Current computer-aided drug design. 2011 Jun 1;7(2):146-57.*
24. Kontoyianni M. *Docking and virtual screening in drug discovery. In Proteomics for drug discovery: Methods and protocols 2017 Aug 15 (pp. 255-266). New York, NY: Springer New York.*
25. Morris GM, Huey R, Lindstrom W, Sanner MF, Belew RK, Goodsell DS, Olson AJ. *AutoDock4 and AutoDockTools4: Automated docking with selective receptor flexibility. Journal of computational chemistry. 2009 Dec;30(16):2785-91.*
26. Kitchen DB, Decornez H, Furr JR, Bajorath J. *Docking and scoring in virtual screening for drug discovery: methods and applications. Nature reviews Drug discovery. 2004 Nov 1;3(11):935-49.*
27. Forli S, Huey R, Pique ME, Sanner MF, Goodsell DS, Olson AJ. *Computational protein–ligand docking and virtual drug screening with the AutoDock suite. Nature protocols. 2016 May;11(5):905-19.*
28. Ylikangas H. *Virtual screening of ligands for kallikrein-related peptidase 3 and the L-type amino acid transporter 1 (Doctoral dissertation, Itä-Suomen yliopisto)*